Materials and Design 175 (2019) 107800

Contents lists available at ScienceDirect

Materials and Design

journal homepage: www.elsevier.com/locate/matdes

Synthesis of colloidal aluminum hydroxide nanoparticles for transparent luminescent polymer nanocomposite films

MinHye Kim [a], Donguk Lee [a], Ho-Young Woo [a], Tae-Hyung Kim [a], Taejong Paik [a,*], Ki-Se Kim [b,*]

[a] Department of Integrative Engineering, Chung-Ang University, Seoul 06974, Republic of Korea
[b] R&D Center, Hanwha Total Petrochemicals, Co., Ltd., Seosan-Si, Chungnam 31900, Republic of Korea

HIGHLIGHTS

- Colloidal luminescent AlOH NPs are synthesized *via* the thermal decomposition of aluminum acetate in the presence of oleic acid.
- Colloidal AlOH NPs are highly dispersible in non-polar solvents and form transparent composites with EVA copolymers.
- AlOH/EVA films exhibit a high PLQY of more than 50%, while maintaining more than 94% of transparency at 600 nm.

GRAPHICAL ABSTRACT

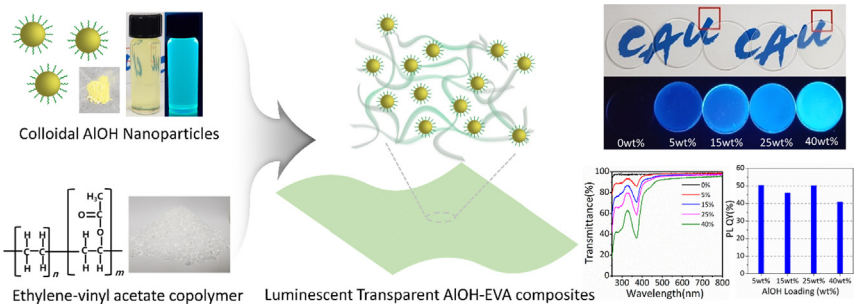

ARTICLE INFO

Article history:
Received 5 December 2018
Received in revised form 13 April 2019
Accepted 15 April 2019
Available online 16 April 2019

Keywords:
Aluminum oxide
Aluminum hydroxide
Nanophosphor
Spectral converter

ABSTRACT

Luminescent inorganic phosphors are widely used as wavelength-converting materials in many emerging applications including displays, solar cells, and bioimaging. This study demonstrates the synthesis of highly luminescent colloidal AlOH nanoparticles and the preparation of transparent luminescent AlOH/polymer composites. Colloidal AlOH nanoparticles are synthesized by the thermal decomposition of aluminum acetate hydroxide precursors in octadecene solution. The addition of oleic acid in the reaction mixture enables the control of the size and dispersity of the nanoparticles. As-synthesized nanoparticles are colloidally stable in non-polar solvents and exhibit excellent photoluminescence properties. Highly dispersible colloidal AlOH nanocrystals form stable mixtures with ethylene vinyl acetate (EVA) copolymers. Transmittance and photoluminescence measurements of the AlOH/EVA composite films when varying AlOH loading demonstrate that the transparent and luminescent AlOH/EVA composite films are promising candidates for applications in spectral converters.

1. Introduction

Luminescent inorganic phosphors as spectral converters, which convert absorbed photons to other useful wavelength ranges, have been widely used for light-emitting diodes [1–3] and solar energy conversions [4–8]. Recently, inorganic nanoparticles such as quantum dots [9,10] and nanophosphors [11–13] have attracted much attention for their applications as spectral converters owing to their unique optical properties. Their absorption and emission wavelengths are readily tunable by changing their size, shape, and composition of inorganic nanocrystals [14–16], which allows efficient spectrum management. In addition, inorganic nanoparticles exhibit high photoluminescence quantum yield (PL QY); for example, semiconducting quantum dots exhibit a PL QY higher than 70% [17]. Compared with organic dyes,

* Corresponding authors.
E-mail addresses: paiktae@cau.ac.kr (T. Paik), kisepro.kim@hanwha-total.com (K.-S. Kim).

https://doi.org/10.1016/j.matdes.2019.107800

luminescent inorganic nanoparticles have high resistance to photobleaching and superior thermal stability without structural degradation [17,18]. For applications in spectral conversion, inorganic/polymer composites are widely utilized by embedding luminescent nanoparticles in a polymeric matrix [19,20]. A polymeric matrix offers superior processability, flexibility, and long-term stability of optical properties [21,22]. Mechanical properties may also be reinforced by synergistic interaction with nanoparticles [23,24]. For this application, a high dispersity of nanocrystals in a solvent or polymeric matrix is essential since poor dispersion of nanocrystals in polymer films results in phase aggregation or precipitation [25–27], which makes it difficult to fabricate large-area and uniformly dispersed luminescent films [22,28]. In addition, designing highly transparent and luminescent polymeric composite films is particularly important for emerging applications such as luminescent downshifting materials for displays [29], solar cells [30,31], and luminescent solar concentrators [32,33]. In order to fabricate transparent and luminescent inorganic-polymeric composites films, it is prerequisite to develop a synthetic method to tune the dispersion of nanoparticles in the solution or polymeric matrix.

Among various luminescent inorganic materials, aluminum hydroxide (AlOH) nanoparticles have a potential for utilization as spectral converters [34]. AlOH exists in various compositions and crystal structures such as aluminum trihydroxides, aluminum monohydroxide, and aluminum oxide, and all of these structures are collectively referred to as AlOH [35]. Aluminum oxide/hydroxide-based materials are cheap and earth-abundant with high stability and are widely used in many commercial applications including catalysts, separation, and optical materials. This material does not contain any heavy metals such as Cd or Pb, which avoids potential environmental concerns. In addition, the blue photoluminescence of Al_2O_3 and γ-AlOOH has been reported in many studies [36–39], which has been attributed to emission from anionic vacancies (F- or F+-centers) under ultra-violet excitation [40–42]. Recent studies have shown that AlOH synthesized by solvothermal reaction exhibits strong photoluminescence properties with high quantum yields owing to the presence of oxygen vacancies and carbon doping [35,43], which makes AlOH an ideal material for luminescent phosphors. However, colloidal AlOH, which exhibits a high PL QY as well as high dispersity in a polymeric matrix, is rarely reported. Aggregation of the nanoparticles in polymer nanocomposites results in the loss of transparency of composite films due to the scattering of light [44]. Therefore, in order to minimize the aggregation of luminescent AlOH nanocrystals and to fabricate large-area, homogeneously dispersed, luminescent polymer nanocomposites, it is important to develop a synthetic method to control the size and dispersity of highly luminescent AlOH nanocrystals.

In this study, we demonstrate the size-controlled synthesis of luminescent AlOH nanocrystals and fabrication of transparent luminescent nanocomposite films. The size and dispersity of AlOH nanocrystals are controlled by adding oleic acid (OA) during the reaction. As-synthesized AlOH nanocrystals exhibit outstanding colloidal stability in non-polar solvents while maintaining excellent photoluminescence properties. The structure is characterized using X-ray diffraction (XRD), X-ray photoelectron spectroscopy (XPS), and Fourier-transform infrared spectrometry (FT-IR). Highly dispersible colloidal AlOH nanocrystals form stable mixtures with ethylene vinyl acetate (EVA) copolymers. We fabricate AlOH/EVA copolymer films and tailor the optical and photoluminescent properties of AlOH/EVA films by varying the loadings of luminescent AlOH in EVA composite films. Transparent and luminescent AlOH/EVA films are potentially applicable in spectral converters for solar photovoltaics and luminescent solar concentrators [32].

2. Methods

2.1. Chemicals

Aluminum diacetate hydroxide, oleic acid (Tech, ≥90%), and chlorobenzene (≥99.5%) were purchased from Sigma-Aldrich. 1-octadecene (90%) was purchased from Acros Organics. Ethylene-vinyl acetate (28 wt% of vinyl acetate) was supplied by Hanwha Total Petrochemicals Co., Ltd. All chemicals were used without any further purification.

2.2. Synthesis of luminescent AlOH nanocrystals

To a 125 mL three-neck flask, 0.8105 g of aluminum diacetate hydroxide, 40 mL of octadecene (ODE), and different amounts of OA (0 mL, 0.25 mL, 0.5 mL) were added. The reaction mixtures were dried under vacuum at 120 °C for 1 h to remove moisture. Then, the reaction was conducted at 320 °C under a nitrogen atmosphere. The maximum temperature was maintained for 4 h. Purification was conducted using toluene and methyl alcohol; the synthesized nanocrystals were collected using a centrifuge at 6000 rpm for 2 min. The purification process was repeated twice and the collected nanocrystals were finally dispersed in toluene.

2.3. Preparation of AlOH/EVA films

To 3 mL of chlorobenzene, 0.3 g of ethylene-vinyl acetate (28 wt% of vinyl acetate) and AlOH nanoparticles (0.016 g, 0.053 g, 0.1 g, 0.2 g) were added, following which the solution was stirred at 80 °C until the EVA polymers were completely dissolved. AlOH/EVA films were prepared by drop-casting of the solution on the quartz substrate and the solution was dried at 50 °C to form composite films on the substrates.

2.4. Characterization

Transmission electron microscopy (TEM) images were recorded using a JEOL JEM-2100 operating at 200 kV. X-ray diffraction measurements were conducted using a Bruker-AXS New D8-Advance. FT-IR spectra were collected using a Thermo Scientific Nicolet 6700. X-ray photoelectron spectroscopy (XPS) measurements were performed using a ThermoFisher Scientific K-alpha. Absorption and transmission spectra were taken on a JASCO V-770 spectrometer. The AlOH-B and AlOH-0.25OA powders were mixed with KBr (5 wt%) and their absorption spectra were recorded using a diffuse reflectance accessory. Photoluminescence (PL) emission and excitation spectra were collected using a Horiba Fluorolog3. PL decay curves were obtained using a single-photon-counting PMT with a 374-nm pulsed laser diode. Absolute PL QY values were measured on the same system using an integrating sphere.(refer to the Supporting Information for details) Total transmittance and total reflectance were recorded using a JASCO V-770 spectrometer with an integrating sphere.

3. Results and discussion

Luminescent AlOH nanocrystals are synthesized *via* the high-temperature thermal decomposition of aluminum acetate precursors, as reported in previous literature [35]. The mixed solution of precursors with octadecene (ODE) is dried under vacuum at 120 °C for an hour. In this stage, the reaction solution looks opaque since the aluminum precursors are not dissolved in the ODE. As the temperature increases, the solution gradually becomes transparent, which indicates the dissolution of the precursors in the ODE solvent. When the temperature reaches about 270 °C, the solution turns transparent yellow, which may have been the starting point of precursor decomposition. In the absence of any surfactants, the reaction mixture turns opaque again during the reaction at 320 °C, which indicates the formation of AlOH particles.

We observed that the addition of OA dramatically affects the size and colloidal stability of the AlOH nanocrystals. OA surfactants have long alkyl chains with carboxylic acid groups at the end, which can act as an anchor to coordinate with a metal ion. Therefore, surfactants added into the reaction mixture can interact with the metal ions exposed on

the surfaces of nanocrystals *via* coordination bonds, which enables the control of the growth rate of the nanocrystals during the reaction [45]. In addition, the long alkyl chain on the surface provides colloidal stability *via* interaction between long hydrocarbon chains and the non-polar solvent [46]. Fig. 1 displays photographs of AlOH nanocrystals in a hexane solution. In the absence of OA, as-synthesized AlOH microparticles (AlOH-B) shows poor colloidal stability in the solvents; thus, AlOH particles are precipitated in the solution (Fig. 1a). Bulk aggregates of AlOH are observed in the TEM image (Fig. 1b). With the addition of 0.25 mL of OA (AlOH-0.25OA), the dispersity of AlOH in the solvent increased, although the solution still looks opaque at high loading, as observed in Fig. 1a. When 0.5 mL of OA is added to the reaction (AlOH-0.5OA), a decrease of particle size is observed, as displayed in Fig. 1d. AlOH-0.5OA nanocrystals form a transparent solution with excellent colloidal stability in non-polar solvents such as hexane, toluene, and chloroform, which may be attributed to the presence of OA on the surfaces of nanocrystals and the decrease of nanocrystal size.

The structure is characterized by powder X-ray diffraction (PXRD) measurements. Fig. 2a displays the PXRD spectrum of AlOH-0.5OA. Broad diffraction patterns with peaks at 19.60° and 40.07° reveal that the synthesized nanoparticles are amorphous structures of aluminum hydroxide [35]. In addition, weak diffraction peaks corresponding to triclinic Al_2O_3, tetragonal Al_2O_3, and trigonal $Al(OH)_3$ phases are also observed, which indicates that relatively small amounts of crystalline phases co-exist with the amorphous phase in the nanoparticles. XPS measurements show the characteristic peaks of the elements including Al 2p, Al 2s, O 1s, and C 1s (Fig. 2b). A high-resolution XPS spectrum of Al 2p is deconvoluted into two peaks, 74.8 eV and 76.9 eV, corresponding to Al—O and Al—OH peaks, respectively; this indicates the formation of AlOH nanoparticles (Fig. 2c). The high-resolution XPS O 1 s band consists of two peaks located at 530.1 eV and 531.9 eV (Fig. 2d). These peaks represent —OH and C═O functional groups, respectively, originating from the presence of the carboxyl functional group (COOH) [35]. In the C 1s band of the XPS spectrum, the peak is deconvoluted into three peaks (Fig. 2e). Peaks located at 284.6 eV and 287.6 eV correspond to C—C groups from the oleic acid surfactants and the C═O group of the carboxylic group on the AlOH surface, respectively. The peak located at 290.7 eV on the C 1s band corresponds to π-π* bonding. This is attributed to the presence of oleic acid on the surfaces since the oleic acid contains a C═C double bond in the middle of a hydrocarbon chain. The presence of OA is also confirmed by FT-IR analysis. Fig. 2f displays the FT-IR spectra of AlOH-0.5OA nanoparticles synthesized with and without OA. Characteristic peaks at 1019, 896, and 527 cm^{-1} are observed, which may be attributed to the vibration of the Al—O group [47]. Symmetric and asymmetric vibration peaks of the COO^- group are also observed at 1585 and 1485 cm^{-1}, indicating the presence of a carboxylate group. Compared to AlOH-B, more intense C—H vibration peaks at 2923 and 2853 cm^{-1} are observed from AlOH-0.5OA nanoparticles, which indicates the presence of OA on the AlOH-0.5OA nanoparticles which provides colloidal stability in the non-polar solvents.

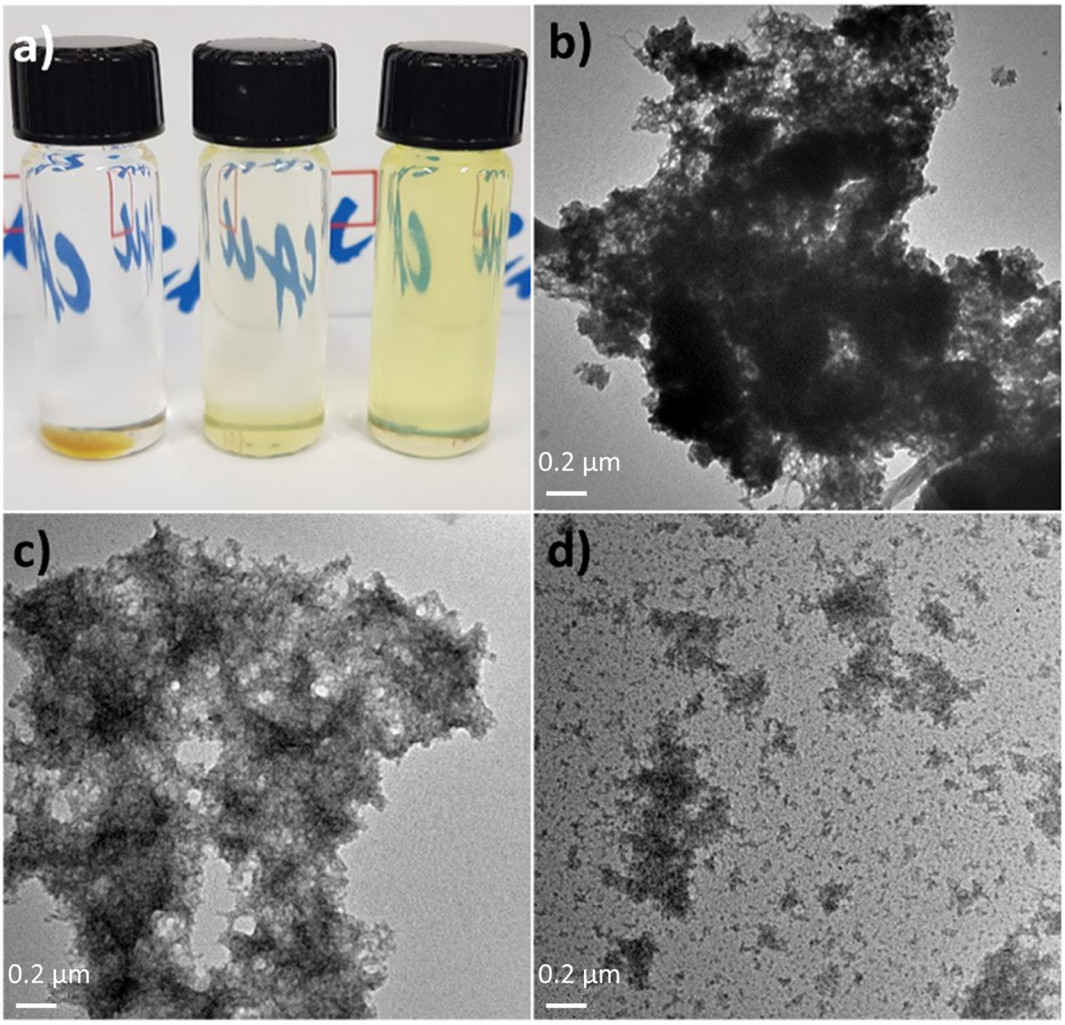

Fig. 1. a) Photograph of AlOH synthesized without OA (left, AlOH-B), with 0.25 mL of OA (middle, AlOH-0.25OA), and 0.5 mL of OA (right, AlOH-0.5OA). AlOH nanoparticles were dispersed in toluene and placed in 4 mL vials. The photo was taken 1 h after sonication. TEM images of b) AlOH-B, c) AlOH-0.25OA, and d) AlOH-0.5OA nanoparticles.

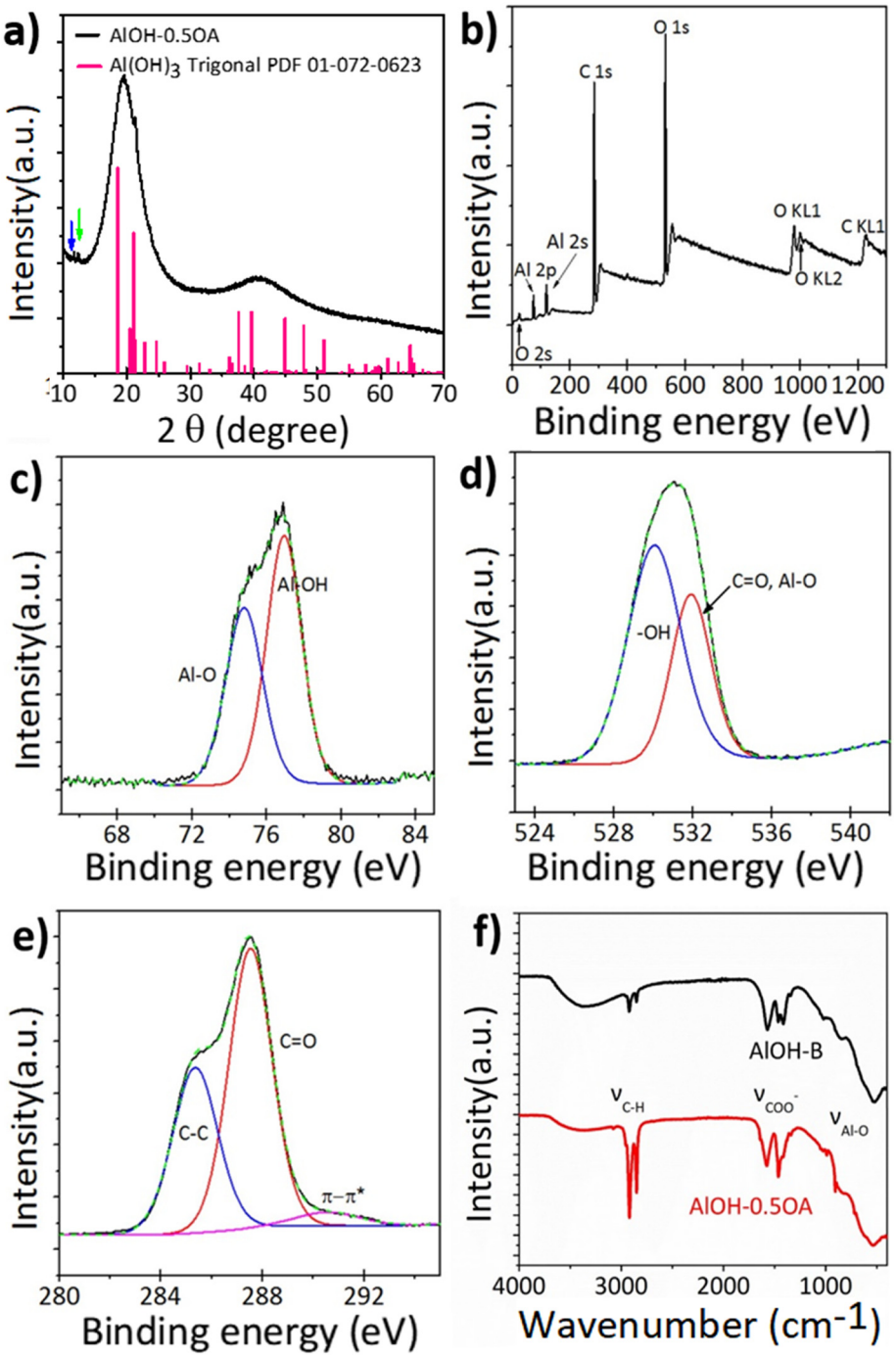

Fig. 2. a) XRD patterns of AlOH-0.5OA nanoparticles. Blue and green arrows represent Al_2O_3 tetragonal (PDF 00-016-0394) and Al_2O_3 triclinic (PDF 01-076-3264), respectively. b) XPS spectra of AlOH-0.5OA nanoparticles. High-resolution XPS of d) Al 2p, d) O 1s and e) C 1s spectra. f) FT-IR spectra of AlOH-B powder and AlOH-0.5OA nanoparticles.

Colloidal AlOH nanoparticles exhibit bright photoluminescent properties. Fig. 3a displays the photoluminescence of AlOH-B, AlOH-0.25OA, and AlOH-0.5OA nanoparticles in toluene. Greenish-blue emission is observed under 365 nm of UV irradiation. In contrast to AlOH-B and AlOH-0.25OA nanoparticles, AlO-0.5OA particles are dispersed in the toluene without the precipitation of nanoparticles; therefore, uniform photoluminescence is observed for the solution. UV-VIS spectra indicates that all samples show absorption peaks located at 370 nm and 440 nm (Fig. 3b). Fig. 3c shows the photoluminescence spectra for AlOH nanoparticles. Characteristic emission peaks at 388 nm and 453 nm are observed from AlOH-B, which is attributed to emission from F^+ centers and carbon-related defects, respectively. [35,48] In the presence of OA, emission peaks are slightly red-shifted to 400 nm/460 nm (AlOH-0.25OA) and 405 nm/460 nm (AlOH-0.5OA), which may be attributed to the presence of OA on nano-sized AlOH, which influences the electronic states of the F^+ centers and carbon-related defects. Excitation spectra exhibited characteristic peaks identical to the absorption spectra (Fig. S1). The absolute photoluminescence quantum yield (PL QY) of AlOH-B is about 37.9%, which is similar to those of bohemite or aluminum hydroxide reported previously [34]. AlOH-0.25OA and AlOH-0.5OA nanoparticles have corresponding values of 40.3% and 36.5% under 370 nm of excitation, which is similar to the value of AlOH-B (37.9%). Under 440 nm of excitation, the PL QY values of AlOH-B, AlOH-0.25OA, and AlOH-0.5OA is 49.4%, 42.29%, and

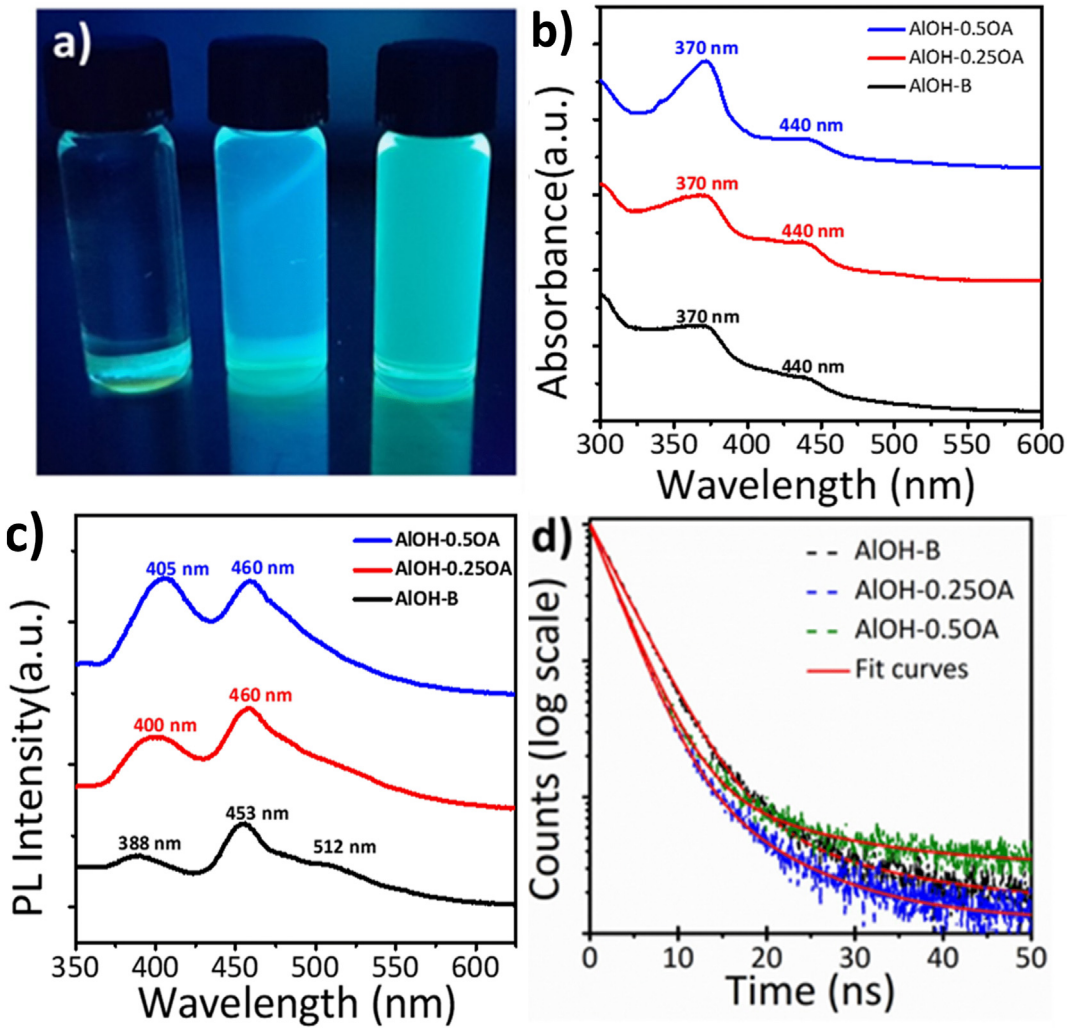

Fig. 3. a) Photographs of AlOH-B (left), AlOH-0.25 (middle), and AlOH-0.5OA (right) under 365-nm excitation. AlOH nanoparticles were dispersed in toluene and placed in 4 mL vials. b) Absorption, c) Photoluminescence, and d) Photoluminescence decay curves of AlOH-B, AlOH-0.25OA, and AlOH-0.5OA nanoparticles.

44.0%, respectively. The deviation of PL QY among the samples is within 5%. The PL QY values of the AlOH nanoparticles and those reported previously in the literature are listed in Table 1. This indicates that addition of OA during the synthesis controls the size of nanoparticles and dispersity in the solution while maintaining high emission quantum yields and strong luminescence properties. Photoluminescence decays are monitored at 470 nm under 374 nm of excitation. Fitting results are tabulated in Table S1. All decay curves of AlOH samples are fitted by bi-exponential functions corresponding to two possible radiative recombination pathways from F^+ centers and carbon-related defects. Radiative lifetimes of the AlOH nanoparticles synthesized with OA and without OA exhibit similar values, which indicates that the addition of OA significantly enhances the colloidal stability of AlOH nanoparticles without deterioration of their optical properties.

Since AlOH nanoparticles are highly dispersible in a non-polar solvent, the nanoparticles form transparent composite films with EVA copolymers. EVA composites are prepared by dissolving AlOH and EVA in chlorobenzene solution with different loadings of nanoparticles and drop-castings on the fused quartz substrates. Owing to the presence of oleic acid on the surface of AlOH nanoparticles, the AlOH nanoparticles and EVA polymers are homogeneously dispersed in chlorobenzene solution and remain as a stable dispersion without precipitation for several months. The mixture of AlOH and EVA is evenly dispersed on the substrate after spin-coating of the solution, resulting in uniform thin films. FT-IR spectra show the characteristic vibrations of the AlOH nanoparticles and EVA polymers in the composite films (Fig. S2). Fig. 4a displays the photograph of the AlOH/EVA composite films under ambient light and UV irradiation. AlOH/EVA composite films maintained transparencies comparable to those of pure EVA films while fluorescence intensities are enhanced owing to the increase of AlOH-0.5OA loading. Fig. 4b shows the total transmittance of the EVA and AlOH/EVA composite films. The transmittance of EVA films from 500 nm to the UV region decreases with an increasing amount of AlOH-0.5OA loaded in the films owing to absorption by AlOH nanoparticles. The total transmittance of the nanocomposite films is above 94% at 600 nm, regardless of the loading of AlOH nanoparticles in composite films. (Fig. 4b) In addition, the total reflectance spectra of the AlOH-EVA nanocomposite films exhibit similar scattering properties as the EVA-only film (Fig. S3); this is attributed to the high dispersion of AlOH nanoparticles in the polymeric matrix. We investigate the photoluminescence properties of AlOH/EVA composite films. Fig. 4c displays absolute PL QY values of AlOH/EVA

Table 1
PL QY values of AlOH-B, AlOH-0.25OA, AlOH-0.5OA, and AlOH. Previously reported PL QY values of bohemite and aluminum hydroxide are 38% and 32–65%, respectively. (Adapted from references [29,30]).

Excitation wavelength	AlOH-B	AlOH-0.25OA	AlOH-0.5OA
370 nm	37.9%	40.3%	36.5%
440 nm	49.4%	42.29%	44.0%

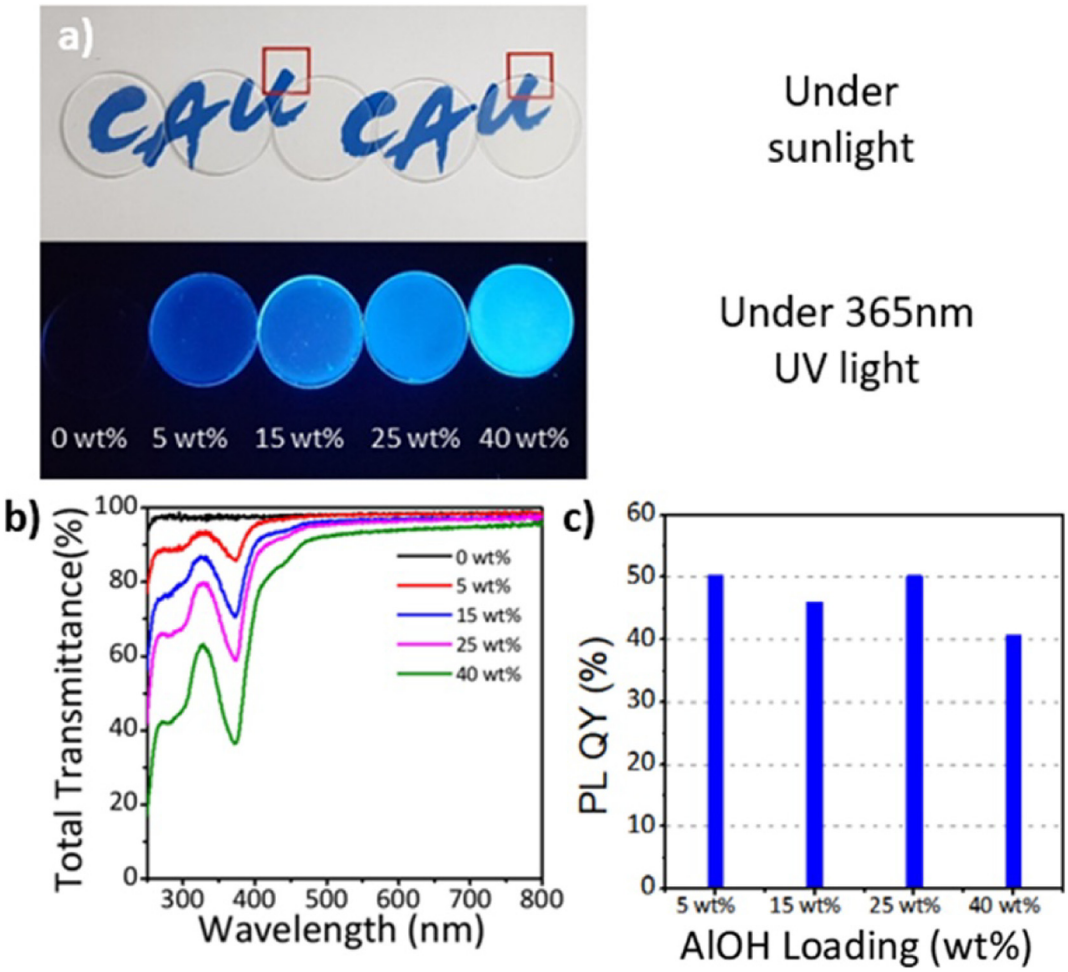

Fig. 4. a) Photographs of AlOH-0.5OA/EVA composite films on a quartz substrate under sunlight (top) and under 365 nm excitation (bottom). The diameter of the quartz substrate is 2 cm. b) Total transmittance spectra and c) absolute PL QY of AlOH-0.5OA/EVA composite film with different AlOH loadings. For PL QY measurement, a wavelength of 370 nm was used for excitation.

composite films with different loadings of AlOH nanoparticles. PL QY values higher than 50% are achieved with 5 wt% and 25 wt% AlOH loadings in EVA films (Table S2). We observe that higher loadings of AlOH nanoparticles up to 40 wt% result in decreased PL QY. Since the absorption and emission spectra of AlOH overlap, a diluted dispersion of AlOH in the polymeric medium may be helpful in preventing the reabsorption of the emitted photons from the nanoparticles, resulting in enhanced QY. High transparency and absolute PL QY reveals that AlOH/EVA composite films have the potential to be utilized as transparent and luminescent spectral converters for applications in photovoltaics and displays.

4. Conclusion

We demonstrate the colloidal synthesis of luminescent dispersible AlOH nanoparticles. The size and dispersity of the AlOH nanoparticles are controlled by changing the amount of OA added to the reaction mixture. As-synthesized AlOH nanoparticles exhibit excellent colloidal stability in non-polar solvents. A high absolute PL QY of AlOH is achieved while maintaining colloidal stability. Tailoring the dispersion of nanoparticles by simply adding OA during the reaction enables us to design highly transparent and luminescent AlOH/EVA copolymer films. The total transmittance at 600 nm is 94%, which is attributed to the high dispersion of AlOH nanoparticles in the polymeric matrix. The absolute PL QY of AlOH/EVA composite films maintains a high value of >50% in 5 wt % and 25 wt% AlOH loadings in EVA films, which confirms that AlOH is inexpensive, earth-abundant, and environmentally friendly luminescent materials with high photoluminescence properties. High transparency and quantum yield enable AlOH/EVA composite films to be attractive candidates for spectral converters for applications in photovoltaics, luminescent solar concentrators, and displays.

Author contributions

The manuscript was written through contributions of all authors. All authors have given approval to the final version of the manuscript.

CRediT authorship contribution statement

MinHye Kim: Investigation, Validation, Visualization, Writing - original draft. **Donguk Lee:** Investigation, Validation, Visualization. **Ho-Young Woo:** Investigation, Validation, Visualization. **Tae-Hyung Kim:** Supervision, Funding acquisition, Writing - review & editing. **Taejong Paik:** Supervision, Funding acquisition, Writing - original draft, Writing - review & editing. **Ki-Se Kim:** Supervision, Writing - original draft, Writing - review & editing.

Acknowledgements

This research was supported by the Creative Materials Discovery Program through the National Research Foundation of Korea (NRF), funded by Ministry of Science and ICT (NRF-2018M3D1A1059001). This research was supported by a grant from the National Research Foundation of Korea (NRF) (NRF-2016R1C1B1016088) and by the Nano

Material Technology Development Program through the NRF of Korea funded by the Korea Government (MSIP) (NRF-2014M3A7B4051907).

Appendix A. Supplementary data

Supplementary data to this article can be found online at https://doi.org/10.1016/j.matdes.2019.107800.

References

[1] H.A. Höppe, Recent developments in the field of inorganic phosphors, Angew. Chem. Int. Ed. 48 (20) (2009) 3572–3582.
[2] N.C. George, K.A. Denault, R. Seshadri, Phosphors for solid-state white lighting, Annu. Rev. Mater. Res. 43 (2013) 481–501.
[3] Q. Zhou, L. Dolgov, A.M. Srivastava, L. Zhou, Z. Wang, J. Shi, M.D. Dramic'anin, M.G. Brik, M. Wu, Mn^{2+} and Mn^{4+} red phosphors: synthesis, luminescence and applications in WLEDs. A review, J. Mater. Chem. C 6 (2018) 2652–2671.
[4] B. McKenna, R.C. Evans, Towards efficient spectral converters through materials design for luminescent solar devices, Adv. Mater. 29 (28) (2017), 1606491.
[5] X. Huang, S. Han, W. Huang, X. Liu, Enhancing solar cell efficiency: the search for luminescent materials as spectral converters, Chem. Soc. Rev. 42 (2013) 173–201.
[6] B.M.v.d. Ende, L. Aarts, A. Meijerink, Lanthanide ions as spectral converters for solar cells, PCCP 11 (2009) 11081–11095.
[7] S. Kalytchuk, S. Gupta, O. Zhovtiuk, A. Vaneski, S.V. Kershaw, H. Fu, Z. Fan, E.C.H. Kwok, C.-F. Wang, W.Y. Teoh, A.L. Rogach, Semiconductor nanocrystals as luminescent down-shifting layers to enhance the efficiency of thin-film CdTe/CdS and crystalline Si solar cells, J. Phys. Chem. C 118 (9) (2014) 16393–16400.
[8] J.H. Song, S. Jeong, Colloidal quantum dot based solar cells: from materials to devices, Nano Converg. 4 (2017) 21.
[9] S.M. Geyer, J.M. Scherer, N. Moloto, F.B. Jaworski, M.G. Bawendi, Efficient luminescent down-shifting detectors based on colloidal quantum dots for dual-band detection applications, ACS Nano 5 (7) (2011) 5566–5571.
[10] F. Meinardi, H. McDaniel, F. Carulli, A. Colombo, K.A. Velizhanin, N.S. Makarov, R. Simonutti, V.I. Klimov, S. Brovelli, Highly efficient large-Aea colourless luminescent solar concentrators using heavy-metal-free colloidal quantum dots, Nat. Nanotechnol. 10 (2015) 878–886.
[11] H. Zhu, C.C. Lin, W. Luo, S. Shu, Z. Liu, Y. Liu, J. Kong, E. Ma, Y. Cao, R.-S. Liu, X. Chen, Highly efficient non-rare-earth red emitting phosphor for warm white light-emitting diodes, Nat. Commun. 5 (2014) 4312.
[12] R.T. Wegh, H. Donker, K.D. Oskam, A. Meijerink, Visible quantum cutting in $LiGdF_4$: Eu^{3+} through downconversion, Science 283 (5402) (1999) 663–666.
[13] X. Ye, J.E. Collins, Y. Kang, J. Chen, D.T.N. Chen, A.G. Yodh, C.B. Murray, Morphologically controlled synthesis of colloidal upconversion nanophosphors and their shape-directed self-assembly, Proc. Natl. Acad. Sci. U. S. A. 107 (52) (2010) 22430–22435.
[14] C.B. Murray, C.R. Kagan, M.G. Bawendi, Synthesis and characterization of monodisperse nanocrystals and close-packed nanocrystal assemblies, Annu. Rev. Mater. Sci. 30 (2000) 545–610.
[15] E. Jang, S. Jun, H. Jang, J. Lim, B. Kim, Y. Kim, White-light-emitting diodes with quantum dot color converters for display backlights, Adv. Mater. 22 (28) (2010) 3076–3080.
[16] P.F. Smet, A.B. Parmentier, D. Poelman, Selecting conversion phosphors for white light-emitting diodes, J. Electrochem. Soc. 158 (6) (2010) R37–R54.
[17] C. Xia, J.D. Meeldijk, H.C. Gerritsen, C. de Mello Donega, Highly luminescent water-dispersible NIR-emitting wurtzite CuInS2/ZnS core/shell colloidal quantum dots, Chem. Mater. 29 (11) (2017) 4940–4951.
[18] I.L. Medintz, H.T. Uyeda, E.R. Goldman, H. Mattoussi, Quantum dot bioconjugates for imaging, labelling and sensing, Nat. Mater. 4 (6) (2005) 435.
[19] Y.L. Yang Li, Z. Guo, L. Dong, J. Zheng, C. Chai, N. Chen, Y. Lu, C. Chen, One-step preparation of long-term stable and flexible $CsPbBr_3$ perovskite quantum dots/ethylene vinyl acetate copolymer composite films for white light-emitting diodes, ACS Appl. Mater. Interfaces 10 (2018), 15888−15894.
[20] Z. Wang, Y. Xiong, S.V. Kershaw, B. Chen, X. Yang, N. Goswami, W.-F. Lai, J. Xie, A.L. Rogach, In situ fabrication of flexible, thermally stable, large-area, strongly luminescent copper nanocluster/polymer composite films, Chem. Mater. 29 (2017) 10206–10211.
[21] K. Rajeshwar, N.R.d. Tacconi, C.R. Chenthamarakshan, Semiconductor-based composite materials: preparation, properties, and performance, Chem. Mater. 13 (9) (2001) 2765–2782.
[22] J. Lee, V.C. Sundar, J.R. Heine, M.G. Bawendi, K.F. Jensen, Full color emission from II-VI semiconductor quantum dot-polymer composites, Adv. Mater. 12 (15) (2000) 1102–1105.
[23] R.J. Moon, A. Martini, J. Nairn, J. Simonsen, J. Youngblood, Cellulose nanomaterials review: structure, properties and nanocomposites, Chem. Soc. Rev. 40 (2017) 3941–3994.
[24] S. Kango, S. Kalia, A. Celli, J. Njuguna, Y. Habibi, R. Kumar, Surface modification of inorganic nanoparticles for development of organic–inorganic nanocomposites—a review, Prog. Polym. Sci. 38 (8) (2013) 1232–1261.
[25] H. Yang, Q. Zhang, M. Guo, C. Wang, R. Du, Q. Fu, Study on the phase structures and toughening mechanism in PP/EPDM/SiO_2 ternary composites, Poly 47 (6) (2006) 2106–2115.
[26] M. Tamborra, M. Striccoli, R. Comparelli, M.L. Curri, A. Petrella, A. Agostiano, Optical properties of hybrid composites based on highly luminescent CdS nanocrystals in polymer, Nanot 15 (2004) S240–S244.
[27] D.E. Fogg, L.H. Radzilowski, R. Blanski, R.R. Schrock, E.L. Thomas, Fabrication of quantum dot/polymer composites: phosphine-functionalized block copolymers as passivating hosts for cadmium selenide nanoclusters, Macromolecules 30 (3) (1997) 417–426.
[28] N. Tomczak, D. Janczewski, M. Han, G.J. Vancso, Designer polymer–quantum dot architectures, Prog. Polym. Sci. 34 (2009) 393–430.
[29] J. Prakash, V. Kumar, L. Erasmus, M. Duvenhage, G. Sathiyan, S. Bellucci, S. Sun, H.C. Swart, Phosphor polymer nanocomposite: ZnO: Tb3+ embedded polystyrene nanocomposite thin films for solid-state lighting applications, ACS Appl. Nano Mater. 1 (2) (2018) 977–988.
[30] V. Svrcek, T. Yamanari, D. Mariotti, S. Mitra, T. Velusamy, K. Matsubara, A silicon nanocrystal/polymer nanocomposite as a down-conversion layer in organic and hybrid solar cells, Nanoscale 7 (27) (2015) 11566–11574.
[31] E. Tatsi, G. Griffini, Polymeric materials for photon management in photovoltaics, Sol. Energy Mater. Sol. Cells 196 (2019) 43–56.
[32] F. Meinardi, S. Ehrenberg, L. Dhamo, F. Carulli, M. Mauri, F. Bruni, R. Simonutti, U. Kortshagen, S. Brovelli, Highly efficient luminescent solar concentrators based on earth-abundant indirect-bandgap silicon quantum dots, Nat. Photon. 11 (3) (2017) 177.
[33] F. Meinardi, Q.A. Akkerman, F. Bruni, S. Park, M. Mauri, Z. Dang, L. Manna, S. Brovelli, Doped halide perovskite nanocrystals for reabsorption-free luminescent solar concentrators, ACS Energy Lett. 2 (10) (2017) 2368–2377.
[34] X. Bai, G. Caputo, Z. Hao, V.T. Freitas, J. Zhang, R.L. Longo, O.L. Malta, R.A.S. Ferreira, N. Pinna, Efficient and tuneable photoluminescent boehmite hybrid nanoplates lacking metal activator centres for single-phase white LEDs, Nat. Commun. 5 (2014) 5792.
[35] B. Chen, A.S. Susha, C.J. Reckmeier, S.V. Kershaw, Y. Wang, B. Zou, H. Zhong, A.L. Rogach, Mesoporous aluminum hydroxide synthesized by a single-source precursor-decomposition approach as a high-quantum-yield blue phosphor for UV-pumped white-light-emitting diodes, Adv. Mater. 29 (2017) 1604284.
[36] Z.Q. Yu, C.X. Wang, X.T. Gu, C. Li, Photoluminescent properties of boehmite whisker prepared by sol-gel process, J. Lumin. 106 (2) (2004) 153–157.
[37] A. Ortiz, J.C. Alonso, V. Pankov, D. Albarran, Violet-blue photoluminescence in aluminium oxide films prepared by ultrasonic spray pyrolysis, J. Lumin. 81 (4) (1999) 45–51.
[38] Y. Yamamoto, N. Baba, S. Tajima, Coloured materials and photoluminescence centres in anodic film on aluminium, Nature (London) 289 (1981) 572–574.
[39] X. Wu, S. Xiong, J. Guo, L. Wang, C. Hua, Y. Hou, P.K. Chu, Ultrathin amorphous alumina nanoparticles with quantum-confined oxygen-vacancy-induced blue photoluminescence as fluorescent biological labels, J. Phys. Chem. C 116 (3) (2012) 2356–2362.
[40] Y. Ohta, T. Hayakawa, T. Inomata, T. Ozawa, H. Masuda, A blue photoluminescent nano boehmite prepared by a solvothermal reaction of aluminum hydroxide gel in monoethanolamine at low temperature, Chem. Lett. 46 (2016) 32–34.
[41] K.H. Lee, J.J.H. Crawford, Luminescence of the F Center in Sapphire 19 (1979) 3217 PhRvB.
[42] B.D. Evans, M. Stapelbroek, Optical properties of the F^+ center in crystalline Al_2O_3, PhRvB 18 (1978) 7089.
[43] B. Chen, X. Xu, S. Zou, Y. Wang, B. Zou, H. Zhong, A.L. Rogach, Single source precursor chemical vapor decomposition method to fabricate stable, bright emissive aluminum hydroxide phosphors for UV-pumped white light-emitting devices, Adv. Opt. Mater. 6 (3) (2018) 1701115.
[44] H. Althues, R. Palkovits, A. Rumplecker, P. Simon, W. Sigle, M. Bredol, U. Kynast, S. Kaskel, Synthesis and characterization of transparent luminescent ZnS:Mn/PMMA nanocomposites, Chem. Mater. 18 (4) (2006) 1068–1072.
[45] J. Park, K. An, Y. Hwang, J.-G. Park, H.-J. Noh, J.-Y. Kim, J.-H. Park, N.-M. Hwang, T. Hyeon, Ultra-large-scale syntheses of monodisperse nanocrystals, Nat. Mater. 3 (12) (2004) 891.
[46] S. Sun, C. Murray, Synthesis of monodisperse cobalt nanocrystals and their assembly into magnetic superlattices, J. Appl. Phys. 85 (8) (1999) 4325–4330.
[47] J. Gangwar, B.K. Gupta, P. Kumar, S.K. Tripathi, A.K. Srivastava, Time-resolved and photoluminescence spectroscopy of θ-Al_2O_3 nanowires for promising fast optical sensor applications, Dalton Trans. 43 (2014), 17034.
[48] N. Nagai, F. Mizukami, Properties of boehmite and al_2o_3 thin films prepared from behmite nanofibres, J. Mater. Chem. 21 (2011) 14884–14889.